Biquintic G^2 surfaces

Kęstutis Karčiauskas[a] and Jörg Peters[b]
[a] Vilnius University [b] University of Florida

July 4, 2013

Abstract

This paper gives a construction to complete, at extraordinary points, an otherwise bi-cubic spline surface – so that the resulting surface is curvature continuous everywhere. To fill the n-sided gap in the bi-cubic surface, a cap is constructed from n spline patches, each consisting of 2×2 pieces of polynomial degree bi-5. Particular care is taken to continue the curvature distribution from the bicubic boundary of the gap into the cap, and gently average out such propagated curvature in the neighborhood of the extraordinary point.

1 Introduction

With an emphasis on curvature distribution, we give an algorithm to cap an n-sided hole within a tensor-product spline, degree bi-3 C^2 surface. Our solution uses n spline patches of polynomial degree bi-5 and such that each patch consists of 2×2 pieces as shown in Fig. 1. Given the lower bound on the polynomial bi-degree and corresponding number of polynomial pieces of G^1 constructions, and given the existing constructions for G^2 surfaces (see Section 1.1 below), this construction likely offers the combination of least degree and minimal number of pieces if we want the entire surface to be curvature continuous.

Since we focus on curvature and hence shape, the new bi-5 construction emphasizes gradual distribution of second-order, hence curvature information from the boundary to the center of the cap. In a two-stage process, we first construct a guide surface, then build the final surface, based on that guide. The guide serves as a form of 'pre-conditioning' that determines the overall shape and curvature distribution, while the second stage constructs the actual bi-5 cap that exactly matches the boundary data and enforces curvature continuity. In this second step, extra degrees of freedom are set by referencing the guide surface.

The guide blends position, tangents and curvature, the tensor-border, from the bi-cubic boundary of the gap. The initial focus is on defining an expansion in the neighborhood of the extraordinary point that averages the boundary data. To this end, we fit a C^2 piecewise polynomial $\mathbf{g}^{\triangle}$ of total degree 5. To improve

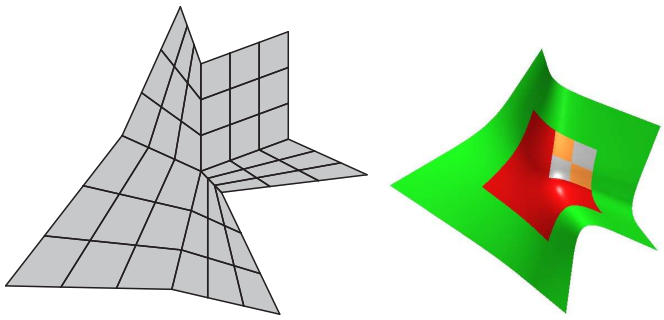

(a) Control net (b) Curvature continuous surface

Figure 1: Converting the neighborhood of a **quad control net into a curvature continuous surface of degree bi-5.** (a) A net of control points with central star point of valence $n = 5$ that defines (b) the outer (green) surface layer of degree bi-3 and the inner (red) cap whose 2×2 pieces are shown for one sector.

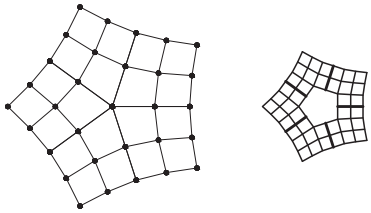

Figure 2: **Input** (*left*) A cap-net for $n = 5$ or, alternatively, (*right*) a corresponding tensor-border of depth 2 represented as BB-form coefficients of degree 3.

the fit to the boundary data, we extend this initial approximation to a guide $\mathbf{g}$ consisting of one polynomial piece of degree bi-5 for each of the n sectors. The guide gives rise to an auxiliary surface $\mathbf{a}$ that has the 'binary' 2×2 partition of each sector, but is not yet smooth between sectors. A final step in the sequence $\mathbf{g}^{\triangle} \rightarrow \mathbf{g} \rightarrow \mathbf{a} \rightarrow \mathbf{p}$ creates the cap $\mathbf{p}$. We demonstrate on a number of examples, that this approach of gentle averaging of boundary data and distributing curvature over the cap results in gradual distribution of curvature.

Overview. Section 2 gives an overview of the construction. Section 3 details the guide construction $\mathbf{g}^{\triangle} \rightarrow \mathbf{g}$. Section 4 specifies the data-independent reparameterizations that ensure G^2 connectivity of the cap. Section 5 gives the construction details: $\mathbf{g} \rightarrow \mathbf{a} \rightarrow \mathbf{p}$. Section 6 treats the spacial case $n = 3$. Section 7 completes the picture with a 'ternary split' variant useful for high valences and to match tensor-borders of degree bi-5. Section 8 presents results and outlines a guided C^2 subdivision based on the guide $\mathbf{g}$. Next, we review the pertinent literature.

1.1 G^2 surface constructions

A good G^2 surface construction has to be flexible to model any and all quadratic and some cubic expansions to match higher-order saddles at its extra-ordinary point – otherwise we would simply extend the boundary data into a plane and generate a flat spot to satisfy smoothness. This basic flexibility requirement implies a minimal degree of general piecewise polynomial surface constructions. For example, flexible G^1 tensor-product n-sided cap constructions for quad meshes with possibly adjacent extraordinary points of valence $n \neq 4$ must have degree bi-3 and 3×3 polynomial pieces per sector if no flat spots are allowed [PF09]. A similar lower bound theorem for G^2 surfaces has not yet been proven, but it appears unlikely that good quality G^2 capping of an n-sided gap in a C^2 bicubic B-spline complex, such as Fig. 1, can be constructed exclusively with polynomial patches of degree bi-4 or by using just one bi-5 patch per sector: The bi-5 construction in [GZ99] is interesting from algebraic point of view, how constraints between sectors are solved, but generally disappoints with respect to shape. [KP07b] has a central cap of degree bi-4 but requires a transition layer of degree bi-6 and the construction [Pet02] of degree 3,5 can have shape defects for moderate to high valence.

Focusing on constructions that use a finite number of tensor-product spline pieces arranged in an unrestricted patch layout, the constructions of [GH95, CNG00, KP04] are high-degree rational and [YZ04, Lev06] use exponential functions and roots. Among polynomial G^2 constructions using a single patch per sector, the degree of can be as high as bi-18 [GH89] and bi-9 [Ye97, Kic13]. The constructions in [Pra97, Rei98] offer solutions of degree bi-6 but only if their flexibility is restricted to degree 2. To attain degree 3 flexibility, the constructions in [Pra97, Rei98] require surfaces of degree bi-9. The constructions of [Loo04, LS08] assume, as does our construction, that surrounding patches are C^2 and of degree bi-3. These constructions explore the space of caps with one polynomial piece of degree bi-7.

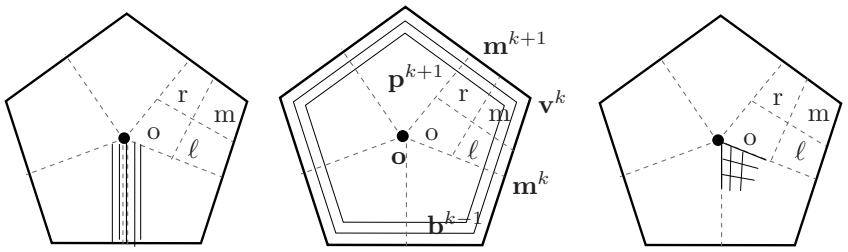

(a) inter-sector: Section 4.1 (b) tensor-border: Section 4.2 (c) Proposition 1

Figure 3: **Algorithm Overview:** Capping an n-sided hole within a bi-3 C^2 surface by n spline patches of 2×2 pieces of polynomial degree bi-5. The pieces (quadrants) of a patch are denoted by superscripts o, ℓ, m, and r. $\mathbf{b}$ denotes the n-sided input tensor-border and $\mathbf{p}$ the output surface cap. The corners of $\mathbf{b}$ are denoted by $\mathbf{v}^k$ and the edge-midpoints by $\mathbf{m}^k$.

To separate *star points* where more or less than 4 patches meet or to reduce the sudden change in curvature at the transition between the cap and the surrounding bi-cubic surface, a number of constructions assume that the input control net is the result of two or more Catmull-Clark refinement steps. Such preprocessing may however itself introduce shape problems due to the dominance of the hyperbolic terms in Catmull-Clark subdivision [KPR04].

Various differential functionals, often linearized, have been proposed to set the degrees of freedom that a smooth surface caps typically enjoy. Since their effect is difficult to predict, we prefer to construct an explicit guiding shape. Already [Pra97, Rei98] introduced a guide polynomial, primarily to ensure C^2 continuity at the extraordinary point of the cap. Entire polynomials were also chosen as 'guide shapes' in [YZ04] and [Lev06] (here the degree of the guide does not play a role since neither scheme generates polynomial or rational surfaces.) However, restricting the guides to be entire polynomials makes the resulting surfaces less expressive and flexible than using piecewise polynomial guides proposed in [Pet02]. The Guided Splines construction [KP09b] specifically advocates the use of piecewise guides for shape control over (global) optimization via functionals.

2 Construction Overview

We consider a network of quadrilateral facets or *quads* such that always four quads meet at a vertex or *regular point*, except for some extraordinary points. We assume that each extraordinary point, abbreviated *eop*, is isolated in the sense that it is surrounded by at least one layer of regular points. We denote as *cap-net* the star point plus the sub-network of $6n$ points forming two layers of quads surrounding the eop. Fig. 2 displays a cap-net and Fig. 1a a cap-net plus one additional layer that is not required, but useful here to define

the (green) surface ribbon surrounding the cap. As in Fig. 1b, away from the star point, each 4×4 tile of points of the network is interpreted as the B-spline control net of a bi-cubic tensor-product spline surface. The well-known conversion formulas of a B-spline control net to Bernstein-Bézier form (*BB-form*; see e.g. [Far02, PBP02]) can be applied to the cap-net except at the central star point. Along the boundary of the cap, the partial conversion provides Hermite data in bi-degree 3 form up to and including the second derivative (cf. Fig. 2,*right*). We refer to these Hermite data in the following as the *tensor-border* $\mathbf{b}$ (of depth 2 and degree 3).

An important concept for determining and controlling shape of the surface cap is the *guide surface*. The guide surface translates the layout and shape of the cap-net into a surface fragment. The guide surface needs neither exactly match the tensor-border nor obey the smoothness constraints.

Since we are interested in G^2 constructions, only position and the first two derivatives across a common boundary curve have to be explicitly defined. In particular, we will match, at corners of tensor-product patches $\mathbf{f}$ of degree bi-5, without loss of generality at $(0,0)$, collections of 3×3 BB-coefficients $\mathbf{f}_{i,j}$, $i,j \in \{0,1,2\}$, referred to as BB-jets:

$$H_{\mathbf{t}}\mathbf{f} := [\mathbf{f}_{ij}]_{i,j\in\{0,1,2\}}, \qquad \mathbf{f}(0,0) = \mathbf{t}. \tag{1}$$

Since the BB-coefficients correspond to the derivatives (the tensor-jet) $\partial_u^i \partial_v^j \mathbf{f}$, $i,j \in \{0,1,2\}$, up to and including degree bi-2, the argument of $H_{\mathbf{t}}$ is allowed to be of lower degree or of higher degree than bi-5. If the degree is lower, 'degree-raising' is applied, if it is higher, the local expansion at $\mathbf{t}$ is recast in degree bi-5 form.

2.1 Capping Algorithm

Input: A cap-net of $6n+1$ points with star point of valence n **or** a tensor-border $\mathbf{b}$ of degree 3 and depth 2 (see Fig. 2).
Data-independent input, that is tabulated for moderate $n < 10$:
Rotation-invariant reparameterization maps $\rho, \beta, \sigma : \mathbb{R}^{2\times n} \to \mathbb{R}^2$.
Output: (see Fig. 1) The surface cap $\mathbf{p}$ consisting of n spline patches $\mathbf{p}^k$, $k = 0, \ldots, n-1$. Patches $\mathbf{p}^{k-1}$ and $\mathbf{p}^k$ are joined G^2 and join with $\mathbf{b}$ both C^1 and G^2. Each $\mathbf{p}^k$ consists of 2×2, C^2-connected polynomial pieces $\mathbf{p}^{o,k}$, $\mathbf{p}^{\ell,k}$, $\mathbf{p}^{m,k}$, $\mathbf{p}^{r,k}$ of degree bi-5.

Algorithm: (see Fig. 3)

1. Construct the guide surface $\mathbf{g}$. The guide $\mathbf{g}$ consists of n C^0-connected pieces of degree bi-5, i.e. a single bi-5 polynomial piece per sector. The guide depends on, but needs not exactly match $\mathbf{b}$ the tensor-border of depth 2 of the cap-net (Fig. 3(b)).

2. Construct the tensor-border of $\mathbf{p}$ to match $\mathbf{b} \circ \beta$.

3. Construct the surface cap $\mathbf{p}$ via an intermediate non-smooth cap $\mathbf{a}$. Determine the free BB-coefficients near the star point by best matching $\mathbf{g} \circ \sigma$ while satisfying the following smoothness constraints.

    1. Adjacent pieces $\mathbf{p}^{k-1}$ and $\mathbf{p}^k$ (cf. Fig. 3(a)) are G^2 connected via ρ.
    2. The cap $\mathbf{p}$ joins $\mathbf{b}$ both C^1 and G^2 (cf. Fig. 3(b)).
    3. The 2×2 polynomial pieces making up $\mathbf{p}^k$ join C^2 internally: $\mathbf{p}^k$ is a C^2 spline patch.

    While the implementation is considerably simpler, deriving it requires constructing in order, as explained in the next three sections, the maps

$$\mathbf{g}^{\triangle} \longrightarrow \mathbf{g} \longrightarrow \mathbf{a} \longrightarrow \mathbf{p}. \tag{2}$$

3 Construction of the guide surface g

The n-piece bi-5 guide surface $\mathbf{g}$ is initialized by an auxiliary C^2 map $\mathbf{g}^{\triangle} : \Omega \subsetneq \mathbb{R}^2 \to \mathbb{R}^3$ of total degree 5 that is defined on the n-gon Ω. The purpose of the map $\mathbf{g}^{\triangle}$ is to average boundary information and define the cap near the star point. The initial cap $\mathbf{g}^{\triangle}$ need not fit the boundary well. A sector $\mathbf{g}^{\triangle k}$ of the map $\mathbf{g}^{\triangle}$ is defined on the wedge

$$\triangle^k \text{ with vertices } (0,0), (\mathsf{c}_k, \mathsf{s}_k), (\mathsf{c}_{k+1}, \mathsf{s}_{k+1}), \tag{3}$$
$$\mathsf{c}_k := \cos(k\frac{2\pi}{n}),\ \mathsf{s}_k := \sin(k\frac{2\pi}{n}).$$

Note the placement of $\mathbf{m}^k$ and $\mathbf{v}^k$ with respect to $\mathbf{g}^{\triangle}$: the corner points $\mathbf{g}^{\triangle k}_{050}$ are edge-midpoints of $\mathbf{b}$. The points $\mathbf{v}^k$ will require an extension of the domain. Fig. 4 shows, as disks and circles, the free BB-coefficients $\mathbf{g}^{\triangle k}_{ijm}$ of any such C^2 map consisting of pieces in BB-form of total degree 5 (cf. Sect 2.3 of [KP09a]; $n = 3, 6$ offer one additional degree of freedom). We set the central point of $\mathbf{g}^{\triangle}$ to the Catmull-Clark limit point of the cap-net and the remaining points $\mathbf{g}^{\triangle k}_{ijm}$ to best match the tensor-border (cf. [KP09b, PK10]) in the sense of matching BB-jets:

$$\min_{\text{free } \mathbf{g}^{\triangle k}_{ijm}} \sum_{k=0}^{n-1} \sum_{\mathbf{t} \in \{\mathbf{m}^k, \mathbf{v}^k\}} \| H_{\mathbf{t}}\big(\mathbf{g}^{\triangle k} \circ \chi\big) - H_{\mathbf{t}} \mathbf{b}^k \|_2^2. \tag{4}$$

Here the tensor-border of the characteristic map (spline) of Catmull-Clark subdivision, $\chi : [0..1]^{2\times n} \to \mathbb{R}^2$, normalized to edge-length 1 (cf. Fig. 6b, *left*, and also Fig. 2, *right*) relates the domain of $\mathbf{g}^{\triangle}$ to n unit squares so that $\mathbf{g}^{\triangle k} \circ \chi^k(1,1) = \mathbf{v}^k$ ($\chi^k(0,0) = (0,0)$, Fig. 5a) and $\mathbf{g}^{\triangle k}_{050} = \mathbf{m}^k$ (Fig. 5b). The auxiliary map $\mathbf{g}^{\triangle}$ determines $\mathbf{g}$ at $\mathbf{o}$ via

$$H_{\mathbf{o}} \mathbf{g}^k := H_{\mathbf{o}}\big(\mathbf{g}^{\triangle k} L\big), \tag{5}$$

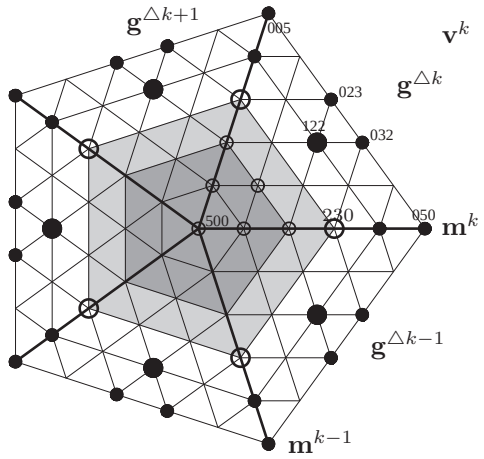

Figure 4: **Structure and labeling of $\mathbf{g}^{\triangle}$**: BB-coefficients marked by circles or disks are free to choose and are set by matching the tensor-border. The remaining BB-control points are determined by the smoothness requirements. Note the placement of $\mathbf{m}^k$ and $\mathbf{v}^k$.

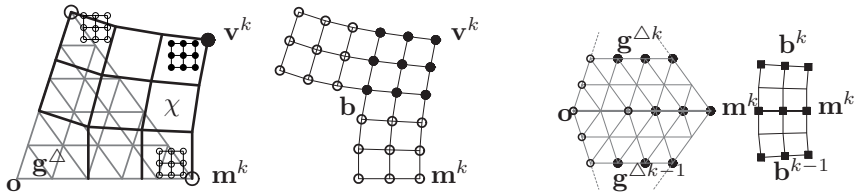

(a) $\mathbf{g}^{\triangle} \circ \chi$-jet matches $\mathbf{b}$-jet at $\mathbf{v}^k$

(b) $\mathbf{g}^{\triangle} \circ \chi$-jet matches $\mathbf{b}$-jet at $\mathbf{m}^k$

Figure 5: **Matching jets.** (a) Matching jets of $\mathbf{g}^{\triangle} \circ \chi$ to those of the tensor-border $\mathbf{b}$. (b) Local exact matching of two pairs of BB-jets. (Note: BB-coefficients denoted by filled circles are different from black disks in (a)).

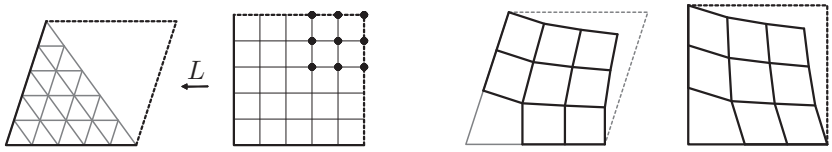

(a) shearing map L

(b) L^{-1} applied to χ

Figure 6: **Linear transformation** of the domain. (a) $\mathbf{g}^{\triangle k} \circ L$ is a bi-5 patch. (b) Transformation of χ.

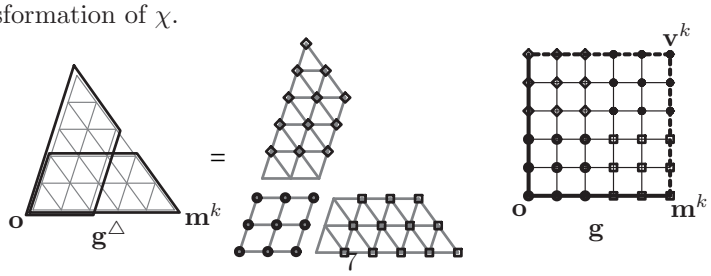

Figure 7: **Separate H-fitting of BB-jets.** The BB-jet of $\mathbf{g}^{\triangle k}L$ at the star point determines the BB-jet of $\mathbf{g}$ at the star point. The remaining coefficients of $\mathbf{g}$ are directly derived from $\mathbf{b}$.

where L is the linear map from the unit square to the unit parallelogram with opening angle $2\pi/n$ (Fig. 6a).

Next, to improve the fit, we *re-compute, locally*, one by one, a part of $\mathbf{g}^{\triangle k-1}$ and $\mathbf{g}^{\triangle k}$ so that

$$H_{\mathbf{m}^k}\big(\mathbf{g}^{\triangle k}\circ\chi\big) = H_{\mathbf{m}^k}\mathbf{b}^k. \tag{6}$$

Fig. 5b illustrates (6): nine BB-coefficients of two pieces of $\mathbf{g}^{\triangle}$ (marked by filled circles) are determined by nine BB-coefficients of $\mathbf{b}$ (marked by black boxes) plus some coefficients of $\mathbf{g}^{\triangle}$ (marked by circles). Not-marked coefficients are determined by enforcing C^2 continuity of $\mathbf{g}^{\triangle}$. Then the corresponding BB-jet of $\mathbf{g}^k$ is

$$H_{\mathbf{m}^k}\mathbf{g}^k := H_{\mathbf{m}^k}\big(\mathbf{g}^{\triangle k}L\big), \tag{7}$$

as illustrated in Fig. 7: for example the BB-jet of $\mathbf{g}^k$ at $\mathbf{m}^k$ that is marked as squares is defined as an affine combination of the twelve BB-coefficient of $\mathbf{g}^{\triangle k}$ in Fig. 7, *middle*, marked by squares. Explicit formulas for the labelled BB-coefficients are simple and do not depend on n. Note that we enforce G^2 constraints between sectors only at the endpoints, $\mathbf{o}$ and $\mathbf{m}^k$, of the sector boundary. That is, we emphasize quality of fit over global smoothness. Finally, we set the remaining free BB-jet of $\mathbf{g}^k$ at $\mathbf{v}^k$ (see Fig. 7,*right*) by solving for the coefficients of $\mathbf{g}^k$

$$H_{\mathbf{v}^k}\big(\mathbf{g}^k L^{-1}\circ\chi\big) = H_{\mathbf{v}^k}\mathbf{b}^k. \tag{8}$$

4 Reparameterizations

It is well-known that C^r continuity of surfaces can be achieved by G^r constructions, i.e. by relating adjacent surface pieces by reparameterization: $\tilde{\mathbf{f}} = \mathbf{f}\circ\rho$. While smoothness of the resulting surface can be expressed in the language of differential geometry, i.e. in terms of charts, it suffices, and is often more efficient, to express the reparameterization locally, as a (Taylor) expansion or jet along the boundary where two surface pieces are glued together. This approach is followed below.

We restrict our attention to polynomial maps, both for reparameterizations and to model the geometry. The polynomial pieces, 2×2 of which make up one C^2 bi-5 spline patch, will be represented in tensor-product BB-form on the unit square $[0,1]\times[0,1]$. Throughout, we will choose the transition boundary to correspond to $(u, v = 0)$ and do not repameterize the boundary. Hence the relevant Taylor expansion up to and including degree 2 of the reparameterization ρ with respect to v is

$$\rho = (u + b(u)v + \frac{1}{2}e(u)v^2, av + \frac{1}{2}d(u)v^2). \tag{9}$$

This yields the well-known constraints

$$\partial_v \tilde{\mathbf{f}} = a\partial_v \mathbf{f} + b(u)\partial_u \mathbf{f}, \tag{G^1}$$
$$\partial_v^2 \tilde{\mathbf{f}} = a^2\partial_v^2 \mathbf{f} + 2ab(u)\partial_u\partial_v \mathbf{f} + b(u)^2\partial_u^2 \mathbf{f} + e(u)\partial_u \mathbf{f} + d(u)\partial_v \mathbf{f}. \tag{G^2}$$

4.1 Reparameterizing between sectors

We assume that the valence of the star point is $n > 3$. The case $n = 3$ will receive special attention in Section 6. Symmetry implies, that the generic formula (9) along the inter-sector boundary becomes (i) $a := -1$ for symmetry at G^1 level and (ii) $e(u) := b(u)\big(b'(u) - \frac{d(u)}{2}\big)$, i.e.

$$\rho = (u + b(u)\big(v + \frac{1}{2}(b'(u) - \frac{d(u)}{2})\big)v^2, -v + \frac{1}{2}d(u)v^2). \tag{10}$$

We choose for the 'top' reparameterization at $\mathbf{o}$ and the 'bottom' reparameterization at $\mathbf{m}^k$ respectively

$$\text{for } \rho^{\mathbf{o}} : b(u) := 2\mathsf{c}(1-u) + \frac{2}{3}\mathsf{c}u,\ d(u) := 0, \qquad \mathsf{c} := \cos\frac{2\pi}{n};$$
$$\text{for } \rho^{\ell r} : b(u) := \frac{2}{3}\mathsf{c}(1-u)^2,\ d(u) := 0.$$

Although $\rho^{\mathbf{o}}$ and $\rho^{\ell r}$ are not C^2-connected, $\mathbf{p}^{\mathbf{o}}$ and $\mathbf{p}^{\ell}$, respectively $\mathbf{p}^{\mathbf{o}}$ and $\mathbf{p}^{r}$ can be constructed to join with C^2 continuity. The major challenge of the construction is the interaction at $\mathbf{m}^k$, especially on the coefficients marked as diamonds in Fig. 8(b). We present the key formulas for enforcing constraints (G^1) and (G^2) and the internal C^2 connection at the star point and at $\mathbf{m}^k$. With the labels of Fig. 8b and abbreviating $\mathbf{q} := \mathbf{p}^{r,k-1}$, $\tilde{\mathbf{q}} := \mathbf{p}^{\ell,k}$, the BB-coefficients (marked in Fig. 8(b) as hollow boxes for (11), respectively as diamonds $\diamond$ for (12)) are

$$\mathbf{q}_{i1} := \mathbf{q}_{i0} + \frac{1}{4}(\mathbf{q}_{i2} - \tilde{\mathbf{q}}_{i2}), \quad \tilde{\mathbf{q}}_{i1} := \mathbf{q}_{i0} - \frac{1}{4}(\mathbf{q}_{i2} - \tilde{\mathbf{q}}_{i2}),\ i = 4, 5, \tag{11}$$

$$\mathbf{q}_{31} := \mathbf{q}_{30} + \frac{1}{4}(\mathbf{q}_{32} - \tilde{\mathbf{q}}_{32}) + w_1(\mathbf{q}_{52} - \tilde{\mathbf{q}}_{52}) + w_2(\mathbf{q}_{42} - \tilde{\mathbf{q}}_{42}) + w_3(\mathbf{q}_{50} - \mathbf{q}_{40}), \tag{12}$$

$$\tilde{\mathbf{q}}_{31} := \mathbf{q}_{30} - \frac{1}{4}(\mathbf{q}_{32} - \tilde{\mathbf{q}}_{32}) - w_1(\mathbf{q}_{52} - \tilde{\mathbf{q}}_{52}) - w_2(\mathbf{q}_{42} - \tilde{\mathbf{q}}_{42}) + w_3(\mathbf{q}_{50} - \mathbf{q}_{40}),$$
$$w_1 := -\frac{\mathsf{c}}{96}, w_2 := \frac{\mathsf{c}}{96}, w_3 := \frac{\mathsf{c}}{30}.$$

Abbreviating $\mathbf{p}_{ij} := \mathbf{p}_{ij}^{\mathbf{o},k-1}$, $\tilde{\mathbf{p}}_{ij} := \mathbf{p}_{ij}^{\mathbf{o},k}$, near the star point $\mathbf{p}_{00}$ (see Fig. 8b),

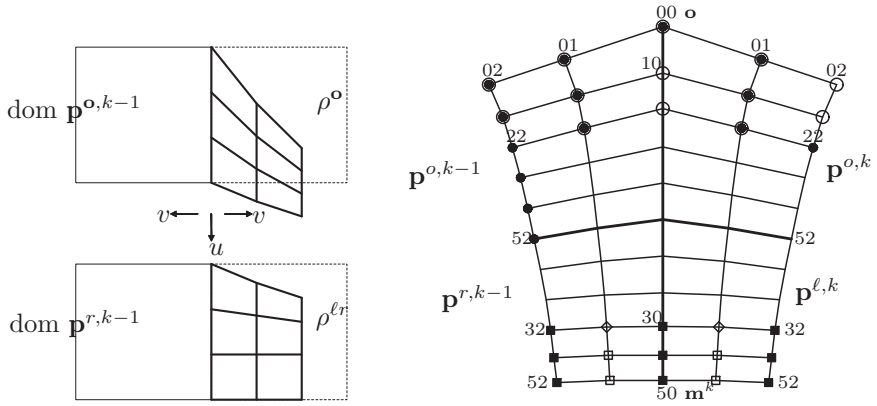

(a) reparameterization ρ (b) BB-coefficients of $\mathbf{p}$

Figure 8: **Inter-sector G^2 constraints.** (a) reparameterizations (top = star point). (b) BB-coefficients of join between sectors: solidly marked coefficients are chosen from data and guide, hollow and unmarked coefficients enforce G^2 continuity. Note that here we chose indices with respect to the sector boundary rather than with respect to rotational symmetry around the star point.

we set

$$\begin{aligned}
\mathbf{p}_{10} :=& \big(1-\frac{1}{\mathsf{c}}\big)\mathbf{p}_{00}+\frac{1}{2\mathsf{c}}(\mathbf{p}_{01}+\tilde{\mathbf{p}}_{01}),\\
\mathbf{p}_{20} :=& \frac{15-26\mathsf{c}+12\mathsf{c}^2}{12\mathsf{c}^2}\mathbf{p}_{00}+\frac{11\mathsf{c}-15}{24\mathsf{c}^2}(\mathbf{p}_{01}+\tilde{\mathbf{p}}_{01})+\frac{5}{8\mathsf{c}}(\mathbf{p}_{11}+\tilde{\mathbf{p}}_{11}),\\
\tilde{\mathbf{p}}_{02} :=& \mathbf{p}_{02}+(2-\frac{5\mathsf{c}}{2})(\tilde{\mathbf{p}}_{01}-\mathbf{p}_{01})+\frac{5\mathsf{c}}{2}(\tilde{\mathbf{p}}_{11}-\mathbf{p}_{11}),\\
\tilde{\mathbf{p}}_{12} :=& \mathbf{p}_{12}-\frac{\mathsf{c}}{6}(\tilde{\mathbf{p}}_{01}-\mathbf{p}_{01})+(2-\frac{11\mathsf{c}}{6})(\tilde{\mathbf{p}}_{11}-\mathbf{p}_{11})+2\mathsf{c}(\tilde{\mathbf{p}}_{21}-\mathbf{p}_{21})\ .
\end{aligned} \tag{13}$$

The remaining formulas for enforcing the constraints (G^1) and (G^2) and the internal C^2 connection express $\mathbf{p}_{ij}$, $i=3,4,5$, $j=0,1$ and $\tilde{\mathbf{p}}_{ij}$, $i=3,4,5$, $j=0,1,2$ in terms of: the unknowns $\mathbf{p}_{i2}$, $i=3,4,5$, the coefficients computed in (11), (12) and the BB-jet of $\mathbf{p}$ at the star point.

4.2 Reparameterizing the tensor-border b

Due to sector-wise symmetry, we need only define reparameterizations $\mathbb{R}^2\to\mathbb{R}^2$ for one sector and rotate by R_n, the rotation by $2\pi/n$. Also note that all reparameterizations are data-independent. They can therefore be computed and tabulated for n once and for all.

To satisfy (11) and (12), we define the reparameterization $\beta:[0..1]^2\to\mathbb{R}^2$ of one sector $\mathbf{b}^k$ of the tensor-border to be the identity up to and including the

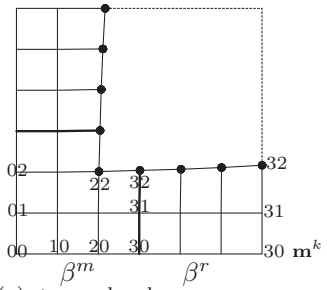

(a) tensor-border reparameterization β

Figure 9: **Transition between bi-3 C^2 surface and the surface cap.** Two piece reparameterization β of the input tensor-border.

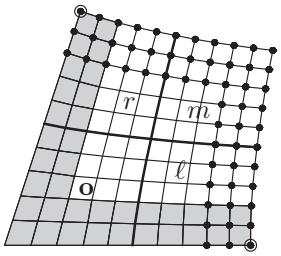

Figure 10: **Structure and labeling of the quadrants** of one sector shared by the spline-patch $\mathbf{p}^k$, the auxiliary patch $\mathbf{a}^k$ and the reparameterization σ. Lower left corner is the star point. BB-coefficients marked as black disks match the tensor-border, BB-coefficients of the grey strips are involved in the inter-sector G^2 constraints.

second cross-derivative along the border of the cap. That is, we set in (9)

$$a := 1, \quad b(u) := 0. \tag{14}$$

Enforcing C^2 continuity internally between the pieces β^m and β^r, and symmetry about the diagonal of β^m (Fig. 9(a)), β is uniquely defined along the tensor-border by the following choice of bi-3 BB-coefficients

$$\beta^m_{22} := \big(\frac{1}{3}+\frac{\mathsf{c}}{216}, \frac{1}{3}+\frac{\mathsf{c}}{216}\big),\ \beta^m_{32} := \big(\frac{1}{2}+\frac{7\mathsf{c}}{1296}, \frac{1}{3}+\frac{\mathsf{c}}{72}\big),\ \beta^r_{32} := \big(1, \frac{1}{3}+\frac{\mathsf{c}}{18}\big). \tag{15}$$

This choice yields the following lemma.

Lemma 1 *The reparameterized tensor-border $\mathbf{b} \circ \beta$ is C^2 within each sector and adjacent pieces $\mathbf{b}^{k-1} \circ \beta$ and $\mathbf{b}^k \circ \beta$ join G^2 according to* (11) *and* (12).

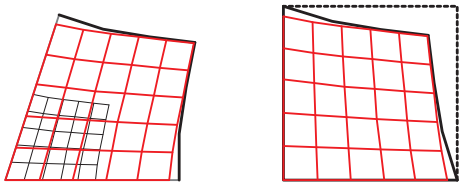

Figure 11: Sampling improved by a **virtual Catmull-Clark subdivision step**.

4.3 Parameterization σ for sampling the guide

We relate $\mathbf{p}^k$ to $\mathbf{g}^k$ via a parameterization $\sigma : \mathbb{R}^2 \to \mathbb{R}^2$ that has the same structure as $\mathbf{p}$: σ is a symmetric planar 2×2 patch of degree bi-5 that matches the tensor-border of χ, reparameterized by β, i.e. the same construction by which $\mathbf{p}$ matches and extends $\mathbf{b}$. The map σ is chosen to be symmetric with respect to its diagonal $u = v$, to match the (equally symmetric) tensor-border of χ (see disks in Fig. 10), to be internally C^2 and to enforce G^2 continuity with $R_n\beta$ using the reparameterization ρ. Points along the boundary must lie on the sector partition lines, and symmetry across the diagonal remove half the degrees of freedom. After enforcing the G^2 constraints (see Fig. 8b) along the inter-sector boundaries, σ has 15 *scalar* parameters to be determined. These are fixed by minimizing (cf. [KP09b])

$$\mathcal{F}_3\sigma, \quad \text{where} \qquad \mathcal{F}_\kappa f := \int_0^1 \int_0^1 \sum_{i+j=\kappa, i,j\geq 0} \frac{\kappa!}{i!j!} (\partial_s^i f \partial_t^j f)^2. \tag{16}$$

This minimization concerns the domain of the final surface, not the surface itself.

5 Assembling p

Section 3 showed how to create the guide $\mathbf{g}$ and Section 4 introduced maps from $\mathbb{R}^2$ to $\mathbb{R}^2$ to allow us to relate the domains of $\mathbf{g}$ and $\mathbf{b}$ to the pieces of $\mathbf{p}$. The BB-coefficients of the expansion at the star point marked by circles in Fig. 8, and at $\mathbf{m}^k$, marked as boxes, are computed first. Then the remaining G^2 and C^2 constraints are enforced.

We start with an auxiliary cap $\mathbf{a}$ of the same degree and layout as $\mathbf{p}$ (see Fig. 10), but not yet G^2 continuous across sector boundaries. The outermost layers with BB-coefficients $\mathbf{a}_{ij}^{s,k}$, $s \in \{\ell, m, r\}$ (see black disks in Fig. 10) match the tensor-border reparameterized by β as detailed in Section 4.2. The four BB-jets at the corners $\mathbf{t}$ of $\mathbf{a}^{o,k}$, the piece nearest $\mathbf{o}$, are defined by

$$H_{\mathbf{t}}\mathbf{a}^{\mathbf{o},k} := H_{\mathbf{t}}\big(C(\mathbf{g})^k \frac{1}{\lambda} L^{-1} \circ \sigma^{\mathbf{o}}\big). \tag{17}$$

Here $C(\mathbf{g})^k$ is the guide obtained by applying one step of Catmull-Clark subdivision to the cap-net to smooth out abrupt transitions in curvature before computing (4) and (7). We counteract this contraction (and do not introduce an extra surface layer) by scaling the parameterization of the new guide with the inverse of the subdominant eigenvalue $\lambda := \frac{1}{16}(\mathsf{c}+5+\sqrt{(\mathsf{c}+1)(\mathsf{c}+9)})$ of Catmull-Clark subdivision (see Fig. 11). We complete $\mathbf{a}$ by connecting $\mathbf{a}^{\mathbf{o},k}$ C^2 to $\mathbf{a}_{ij}^{s,k}$, $s \in \{\ell, m, r\}$.

To obtain a cap that is G^2 also across the sector boundaries $(\mathbf{o}, \mathbf{m}^k)$, we have to correct the BB-coefficients in the n *strips* (underlaid grey in Fig. 10) that define the derivatives up to and including second order across the sector boundaries. Setting, with the indexing of Fig. 8,

$$\mathbf{p}_{ij}^{r,k-1} := \mathbf{a}_{ij}^{r,k-1} \text{ and } \mathbf{p}_{ij}^{\ell,k} := \mathbf{a}_{ij}^{\ell,k},\ i = 3..5, j = 0..2, \tag{18}$$

enforces the G^2 constraints (11) and (12) at $\mathbf{m}^k$ and allows us to focus on the remaining strips

$$\mathbf{P}_K := \{\mathbf{p}_{ij}^{\mathbf{o},k-1},\ \mathbf{p}_{ij}^{\mathbf{o},k},\ i = 0..5, j = 0..2; \mathbf{p}_{ij}^{r,k-1},\ \mathbf{p}_{ij}^{\ell,k},\ i = 0..2, j = 0..2\}_{k=0..n-1}.$$

We enforce G^2 vertex enclosure constraints at the star point by giving to $H_{\mathbf{o}}\mathbf{p}^{\mathbf{o},k}$, $k = 1, \ldots, n$, as degrees of freedom, exactly the $n+6$ BB-coefficients ($n+1+6$ if $n = 6$)

$$G_3 := \{\bar{\mathbf{g}}_{ijm}^{\triangle 1}\}_{i>0} \cup \{\bar{\mathbf{g}}_{030}^{\triangle k}\}_{k=0\ldots n-1} \tag{19}$$

of a C^2 piecewise polynomial $\bar{\mathbf{g}}^{\triangle}$ of degree 3 – shown as circles in the gray region of Fig. 4. That is all BB-jets $H_{\mathbf{o}}\mathbf{p}^{\mathbf{o},k}$ at the star point have the form

$$H_{\mathbf{o}}\big(\bar{\mathbf{g}}^{\triangle k} \circ \sigma^{\mathbf{o}}\big) \tag{20}$$

with $\mathbf{p}_{22}^{\mathbf{o},k}$ still free to choose. After the substitutions derived in Section 4.1 and enforcing the C^2 continuity internal to each $\mathbf{p}^k$, the BB-coefficients of $\mathbf{P}_K$ are expressed in terms of $\mathbf{p}_{i2}^{o,k}$, $i \in \{2,3,4,5\}$ (marked as small black disks $\bullet$ in Fig. 8b), the BB-jet at the star point and the BB-jets at $\mathbf{m}^k$, $\mathbf{p}_{ij}^{r,k-1}$ and $\mathbf{p}_{ij}^{\ell,k}$, $i = 3..5, j = 0..2$. Treating the $4n$ coefficients $\mathbf{p}_{i2}^{o,k}$ together with G_3 of (19) as unknowns, $\mathbf{P}_K$ now depends on $5n+6$ unknowns ($5n+1+6$ unknowns if $n = 6$) that are determined by minimizing

$$\min_{G_3, \mathbf{p}_{i2}^{o,k}} \mathcal{F}_1(\mathbf{p}^{s,k} - \mathbf{a}^{s,k}), \qquad k = 0..n-1,\ i = 2..5,\ s = \{\ell, \mathbf{o}, r\}. \tag{21}$$

We verify the following proposition by substitution.

Proposition 1 *The jets of* $\mathbf{p}^{\mathbf{o},k}$ *computed in* (20) *satisfy* (13).

To summarize, we constructed in order

$$\mathbf{g}^{\triangle} \longrightarrow \mathbf{g} \longrightarrow \mathbf{a} \longrightarrow \mathbf{p}. \tag{22}$$

Since the patches $\mathbf{p}^k$ are constructed to be internally C^2, Proposition 1 and Lemma 1 prove that the cap is curvature continuous and matches the tensor-border with curvature continuity.

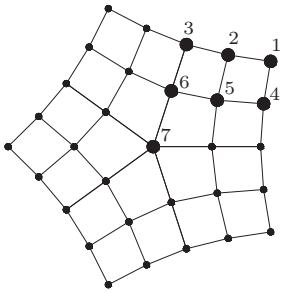

Figure 12: **cap-net-labelling**.

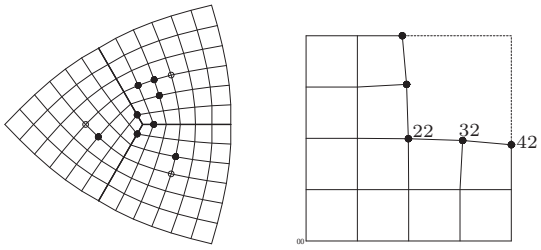

(a) $n = 3$ (b)

Figure 13: (a) Black disks = free points of the bi-6-construction $\mathbf{g}$ near the star point. Circles = unconstrained innermost control points (b) Degree 4 reparameterization ρ of input tensor-border.

5.1 Implementation

We compute, for various n, once and for all, the data-independent reparameterizations β and σ (ρ is not needed in explicit form). The construction is linear and coordinate-wise. Due to the relatively short, explicit formulas for the BB-coefficients of $\mathbf{g}$ and $\mathbf{p}$ in terms of unconstrained BB-coefficients, the construction steps of the Capping Algorithm are stable and fast. The undetermined coefficients of $\mathbf{g}^{\triangle}$ (the star point is fixed) are determined by solving a linear system of size $(6n+5) \times (6n+5)$. Enforcing (21) requires solving a linear system of size $(5n+6) \times (5n+6)$. The implementation is made even more efficient by tabulating seven *generating functions of the cap-net*. Since the Capping Algorithm works for each coordinate separately, it can be applied to when all cap-net points have value 0, except for $\mathbf{c}_m^1 = 1$, for one of $m = 1, \ldots, 7$ (see Fig. 12. This yields the scalar-valued bi-5 coefficients $h_{ij}^{k,m}$, $m = 1, \ldots, 7$, $k = 0, \ldots, n-1$, $i, j \in \{0, \ldots, 5\}$ where $h_{ij}^{1,7} = \ldots = h_{ij}^{n,7}$. Then $\mathbf{p^o}$ has the BB-coefficients

$$\mathbf{p}_{ij}^{o,s} := \sum_{k=0}^{n-1} \sum_{m=1}^{6} h_{ij}^{k,m} \mathbf{c}_m^{s-k} + h_{ij}^{1,7} \mathbf{c}_7^1. \tag{23}$$

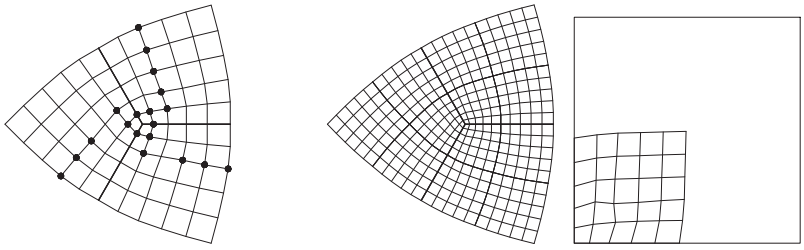

(a) free BB-coefficients (b) σ for $n = 3$ (c) S

Figure 14: (a) Unconstrained BB-coefficients • of $\mathbf{p^o}$ after resolving the smoothness constraints. (b) 'Characteristic' parameterization. (c) Biquintic reparameterization for sampling bi6 guide.

6 Special construction for valence 3

Since a denominator of σ vanishes for $n = 3$, we exploit the special options offered by $n = 3$.

6.1 A G^2 bi-6 guide surface

We construct a G^2 guide surface $\tilde{\mathbf{g}}$ of degree bi-6 with one patch per sector. This guide is by itself a G^2 cap, of lower degree than previous known constructions and good shape, but will be replaced by a bi-5 cap to match the representation in the rest of this paper. We choose $b(u) := -(1-u)^2$, $d(u) := -4(1-u)^2$ for the reparameterization between the patches. Then the tensor-border defines the BB-coefficients $\mathbf{q}_{ij}$ of $\tilde{\mathbf{g}}^k$ and $\tilde{\mathbf{q}}$ of $\tilde{\mathbf{g}}^{k+1}$ so that

$$\mathbf{q}_{i1} := \mathbf{q}_{i0} + \frac{1}{4}(\mathbf{q}_{i2} - \tilde{\mathbf{q}}_{i2}), \quad \tilde{\mathbf{q}}_{i1} := \mathbf{q}_{i0} - \frac{1}{4}(\mathbf{q}_{i2} - \tilde{\mathbf{q}}_{i2}),\ i = 5, 6. \tag{24}$$

$$\mathbf{q}_{41} := \mathbf{q}_{40} + \frac{1}{4}(\mathbf{q}_{42} - \tilde{\mathbf{q}}_{42}) + w_1(\mathbf{q}_{62} - \tilde{\mathbf{q}}_{62}) + w_2(\mathbf{q}_{52} - \tilde{\mathbf{q}}_{52}) + w_3(\mathbf{q}_{60} - \mathbf{q}_{50}),$$

$$\tilde{\mathbf{q}}_{41} := \mathbf{q}_{40} - \frac{1}{4}(\mathbf{q}_{42} - \tilde{\mathbf{q}}_{42}) - w_1(\mathbf{q}_{62} - \tilde{\mathbf{q}}_{62}) - w_2(\mathbf{q}_{52} - \tilde{\mathbf{q}}_{52}) + w_3(\mathbf{q}_{60} - \mathbf{q}_{50}),$$

where $w_1 := \frac{1}{150}$, $w_2 := -\frac{1}{100}$, $w_3 := -\frac{1}{30}$. The remaining unconstrained BB-coefficients are shown as black disks in Fig. 13a.

Similar to the general case, but using just one piece, the degree 6 tensor-border is obtained by reparameterization with a map β of degree 4 (see Fig. 13b). Position and first cross-derivative layers are preserved by (24). The coefficients of β defining G^2 continuity are

$$\beta_{22} := (\frac{287}{576}, \frac{287}{576}),\ \beta_{32} := (\frac{293}{384}, \frac{47}{96}),\ \beta_{42} := (1, \frac{15}{32}). \tag{25}$$

With the outermost layers of $\tilde{\mathbf{g}}$ match the tensor-border, we fix the three neigh-

bors of the star point so that

$$\text{star point} := \sum_{i=0}^{2}\sum_{m=1}^{6} E_m \mathbf{c}_m^i + (1 - 3\sum_{m=1}^{6} E_m)\mathbf{c}_7^1, \tag{26}$$

where $\mathbf{c}$ is defined in Section 5.1 and

$$\begin{aligned} E_1 :=& 0.00004133,\ E_2 = E_4 := 0.00049235,\ E_3 := 0.00079515, \\ E_5 :=& 0.04832434,\ E_6 := 0.16420709 \end{aligned} \tag{27}$$

is obtained by experiment improving on poor results when choosing the limit of Catmull-Clark subdivision. Fixing the star point reduces number of unconstrained BB-coefficients, marked by circles or disks in Fig. 13a. The remaining 10 BB-coefficients are determined by minimizing $\mathcal{F}_4(\tilde{\mathbf{g}}^1) + \mathcal{F}_4(\tilde{\mathbf{g}}^2) + \mathcal{F}_4(\tilde{\mathbf{g}}^3)$. Applying this construction to the symmetric planar input of a degree-raised normalized tensor-border of χ yields the parameterization σ^6 shown in Fig. 13a.

6.2 Reparameterization across sector-boundaries

To have $\mathbf{p}^{r,k-1}$ and $\mathbf{p}^{\ell,k}$ join C^2, we choose

$$\rho^{\mathbf{o}}: \quad b(u) := -(1-u)^3, \quad d(u) := -6(1-u)^3. \tag{28}$$

Fig. 14a shows as black disks the unconstrained BB-coefficients of $\mathbf{p}^{\mathbf{o}}$ after resolving the smoothness constraints over all three sectors and enforcing C^2 continuity within each $\mathbf{p}^k$. The structure of $\mathbf{p}$ is the same as for $n \neq 3$: $\mathbf{b}$ defines the outermost layers of $\mathbf{p}^{\ell,k}$, $\mathbf{p}^{m,k}$ and $\mathbf{p}^{r,k}$. The strips are modified to enforce (28) plus internal C^2 continuity and only the 3×3 collection of BB-coefficients, where the four pieces of a patch meet, is undetermined. Applying this construction to the symmetric planar tensor-border of χ and minimizing $\mathcal{F}_3$ yields σ for $n = 3$, shown in Fig. 14b.

We construct the guiding bi-5 $\mathbf{g}^{\mathbf{o},k}$ by setting

$$H_{\mathbf{t}}\mathbf{g}^{\mathbf{o},k} := H_{\mathbf{t}}\big(\tilde{\mathbf{g}}^{\mathbf{o},k} \circ S\big) \tag{29}$$

where S is a bi-5 reparameterization obtained as follows. We compute numerically the four vertices $\mathbf{v}_{ij} := (\sigma^6)^{-1} \circ \sigma^o(i,j)$, $i,j \in \{0,1\}$ where σ^6 is a 'characteristic' parameterization of degree bi-6 constructed as in the previous section. Then S is defined by the requirement $H_{\mathbf{v}_{ij}}\sigma^o = H_{\mathbf{v}_{ij}}\big(\sigma^6 \circ S\big)$. Analogous to general case, we finally determine $\mathbf{p}$ by minimizing

$$\sum_{k=0}^{2}\sum_{s\in\{\ell,m,r\}} \mathcal{F}_4(\mathbf{p}^{s,k} - \mathbf{g}^{s,k}). \tag{30}$$

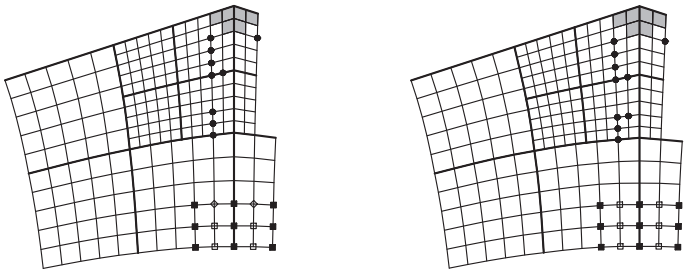

(a) (b)

Figure 15: Degrees of freedom in the G^2 of ternary spline patch: (a) according to (12), (b) according to (34).

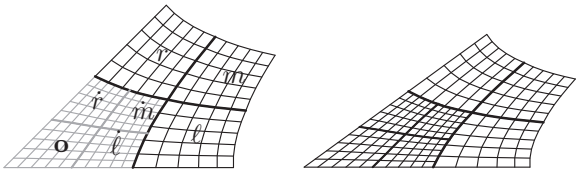

(a) $n = 8$ (b) $n = 10$

Figure 16: Ternary parameterization σ.

7 Ternary-split for high valences

For completeness of discussion and since the curvature distribution can deteriorate for challenging data when $n \geq 8$, we consider a ternary split of each sector into seven C^2-connected patches as shown in Fig. 16 b. Analogous to Catmull-Clark subdivision, it is not necessary to split the outer patches, and create a 3×3 macro patch. Fig. 20 demonstrates the resulting shape improvement for higher valences over the earlier 2×2 spline construction of Section 5.

For the G^2 join between sectors we choose

$$\begin{aligned}
&\text{for } \rho^{\mathsf{o}} : b(u) := \mathsf{c}\sum_{j=0}^{2} b_j^{\mathsf{o}} B_j(u)\ ,\ d(u) := d_0^{\mathsf{o}} + d_1^{\mathsf{o}} u;\\
&\text{for } \rho^{\dot{\mathrm{r}}\dot{\ell}} : b(u) := \mathsf{c}\sum_{j=0}^{2} b_j^{\dot{r}\dot{\ell}} B_j(u)\ ,\ d(u) := d_0^{\dot{r}\dot{\ell}} + d_1^{\dot{r}\dot{\ell}} u;\\
&\text{for } \rho^{\mathrm{r}\ell} : b(u) := \frac{2\bar{Z}}{5}\mathsf{c}B_0(u),\ d(u) := 4Z\mathsf{c}B_0(u), \quad Z := 3z-4,\ \bar{Z} := 2z-1,
\end{aligned} \tag{31}$$

where z is a free parameter, $B_j(u)$ a BB-polynomial of degree 2 and

$$\begin{aligned} b_0^{\mathsf{o}} :=& 2\mathsf{c},\ b_1^{\mathsf{o}} := \frac{1}{5}(4z+3)\mathsf{c},\ b_2^{\mathsf{o}} := z\mathsf{c},\ d_0^{\mathsf{o}} := 6Z\mathsf{c},\ d_1^{\mathsf{o}} := -2Z\mathsf{c}; \\ b_0^{\dot{r}\dot{\ell}} :=& z\mathsf{c},\ b_1^{\dot{r}\dot{\ell}} := \frac{3\bar{Z}}{5}\mathsf{c},\ b_2^{\dot{r}\dot{\ell}} := \frac{2\bar{Z}}{5}\mathsf{c},\ d_0^{\dot{r}\dot{\ell}} := 4Z\mathsf{c},\ d_1^{\dot{r}\dot{\ell}} := -2Z\mathsf{c}. \end{aligned} \tag{32}$$

The G^2 construction connecting to the tensor-border uses

$$w_1 := \frac{\mathsf{c}}{160}(z-3),\ w_2 := \frac{\mathsf{c}}{160}\bar{Z},\ w_3 := \frac{\mathsf{c}}{50}\bar{Z}\ ; \tag{33}$$

which is identical to (11) when $z := \frac{4}{3}$. Fig. 15(a) shows the BB-control points not constrained by the G^2 constraints across sector boundaries. The structure and degrees of freedom in the gray neighborhood of the star point are as in Fig. 8(b), σ is defined via $\mathcal{F}_3$ with $z := \frac{53}{41}$ (see Fig. 16).

The patchworks $\mathbf{p}^{s,k}$ and $\mathbf{a}^{s,k}$ are defined according to Section 5 but minimizing $\mathcal{F}_3$.

7.1 Ternary bi-5 cap matching a degree 5 tensor-border

The extra degrees of freedom can alternatively be used to accommodate tensor-borders of degree 5, as is common in modeling complex shapes and avoids introducing an artificial layer of bi-3 spline patches. Choosing $d(u) := 0$ and

$$\begin{aligned} \rho^{\mathsf{o}}:\ b(u) &:= 2\mathsf{c}(1-u) + \frac{5}{4}\mathsf{c}u; \\ \rho^{\dot{r}\dot{\ell}}:\ b(u) &:= \frac{5}{4}\mathsf{c}(1-u) + \frac{1}{2}\mathsf{c}u, \\ \rho^{r\ell}:\ b(u) &:= \frac{1}{2}\mathsf{c}(1-u)^3. \end{aligned} \tag{34}$$

we obtain one extra degree of freedom (see Fig. 15b) and the constraints at $\mathbf{m}^k$ become the standard C^2 constraints corresponding to $w_1 = w_2 = w_3 = 0$ in (33). Such C^2 constraints allows the cap to continue a tensor-border of degree 5 without reparameterization. However, although we gained one degree of freedom, one degree of freedom is lost in the reparameterizations and the curvature distribution of the construction according to (34) appears to be slightly worse than that according to (31).

8 Results and Discussion

We use basic hard test cases in Fig. 17. Fig. 18 demonstrates high quality for valences $n = 5, 6$ based on the main 'binary split' bi-5 construction. However Fig. 19c hints for $n = 8$ that an improvement may be needed for higher valences and Fig. 20(a),(b) confirms this for $n = 9$.

The 'ternary split' construction carries good quality beyond $n = 7$, up to and including $n = 10$. Beyond that the sectors of the guide $\mathbf{g}$ become so slim

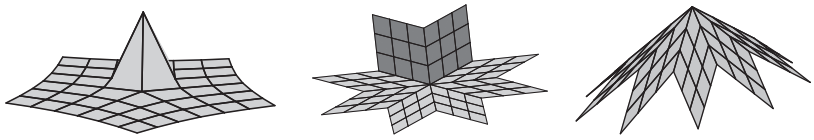

(a) Off-center peak (b) Bent star (c) Convexity test

Figure 17: **Test cases.** (b) planar mesh (light gray) with perpendicular back (dark grey). (c) Convex cap test (that Catmull-Clark-subdivision fails).

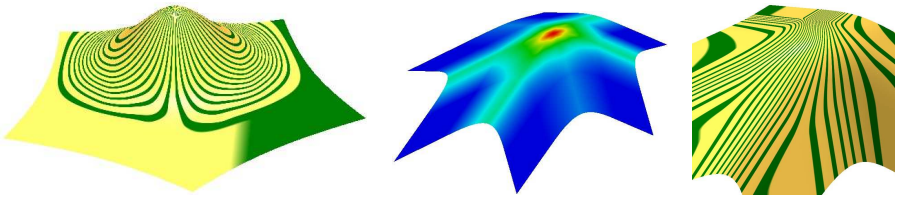

(a) highlight lines (b) mean curvature (c) highlight lines

Figure 18: (a) Input Fig. 17(a). (b,c) Input Fig. 17(c) of valence $n = 6$.

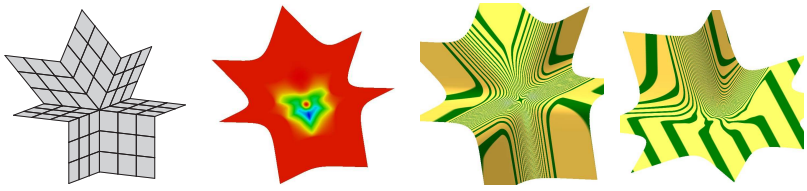

(a) cap-net+layer (b) Gauss curvature (c) highlight lines

Figure 19: Input Fig. 17(b) for valence $n = 7$ (a,b,c) and $n = 8$ (c).

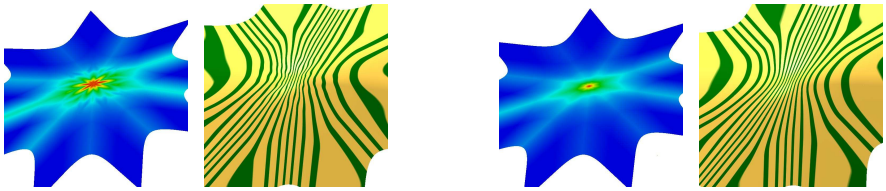

(a) 2×2 spline patch (b) ternary split spline patch

Figure 20: Input Fig. 17(c): Mean curvature and highlight shading.

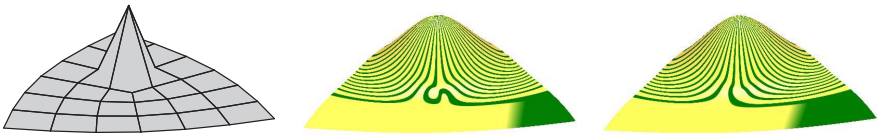

(a) off-center peak (b) $\tilde{\mathbf{g}}$ standard (c) $\tilde{\mathbf{g}}$ using (26)

Figure 21: **Valence $\mathbf{n} = \mathbf{3}$**: (b,c) improvement of highlight lines by choice of star point.

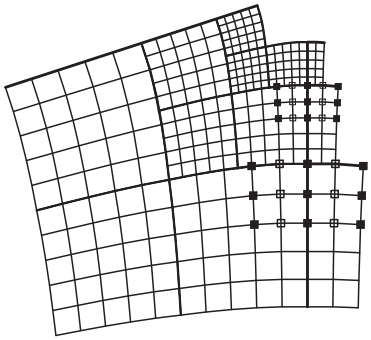

Figure 22: Correction to C^2 of sampled patches in guided subdivision.

and the C^0 junctions so close that we suggest for valences $n > 10$ to use a bi-7 guide that is G^2 between sectors.

At first glance, it seems that using a single patch of degree bi-7 with 64 coefficients per sector of the cap is computationally advantageous. However, since the tensor-border is prescribed, and since our bi-5 construction pins down coefficients by internal C^2 constraints, the actually free BB-coefficients are those of one bi-5 patch per sector, or 36 coefficients. In any case, such simple counting can mislead since the actual implementation involves numerous trade-offs. For example [Loo04, LS08] reparameterize already the first derivative across the boundary between the bi-cubic data and the cap to satisfy algebraic constraints. We found that C^1 continuation yields a better curvature distribution.

8.1 Guided subdivision based on g

Since the b-i5 guide $\mathbf{g}$ plays a crucial role and since $\mathbf{g}$ is curvature continuous at the star point, it is tempting to base a guided subdivision algorithm on $\mathbf{g}$ following [KP07a, PR08]. Applying that approach with patches of degree bi-5 yields a surface that is curvature-bounded at the star point; using patches of degree bi-6 yields C^2 continuity at the star point. The construction is simple, requiring only adjustment of the BB-jets shown in Fig. 22 to make them C^2 (the 'bottom' BB-jets already meet C^2 as C^2 extensions of the preceding subdivision surface ring). While the construction appears simpler, it comes at the usual cost

of rendering recursively generated surfaces.

9 Conclusion

The paper explored the 'guided' approach to creating surfaces with good curvature distribution. The goal was to not abruptly change the curvature distribution across the bicubic boundary of the gap and to gently average out the propagated curvatures in the neighborhood of the star point. Besides the main approach using a 'binary' 2×2 partitioned spline patch, we addressed more challenging data, such as high valence, by a ternary variant, also of degree bi-5. While the constructions appear at first look complex, and indeed their derivation involved challenging symbolic computing, the resulting construction has a simple tabulated representation.

Acknowledgments.

Work supported in part by NSF Grant CCF-1117695.

References

[CNG00] J. Cotrina Navau and N. Pla Garcia. Modelling surfaces from planar irregular meshes. *Comput. Aided Geom. Design*, 17(1):1–15, 2000.

[Far02] G. Farin. *Curves and Surfaces for Computer Aided Geometric Design: A Practical Guide*. Academic Press, San Diego, 2002.

[GH89] John A. Gregory and Jorg M. Hahn. A C^2 polygonal surface patch. *Comp Aided Geom Design*, 6(1):69–75, 1989.

[GH95] C. M. Grimm and J. F. Hughes. Modeling surfaces of arbitrary topology using manifolds. *Computer Graphics*, 29(Annual Conference Series):359–368, 1995.

[GZ99] John A. Gregory and Jianwei Zhou. Irregular C^2 surface construction using bi-polynomial rectangular patches. *Computer Aided Geometric Design*, 16(5):423–435, 1999.

[Kic13] Przemyslaw Kiciak. Spline surfaces of arbitrary topology with continuous curvature and optimized shape. *Computer-Aided Design*, 45(2):154–167, 2013.

[KP04] K. Karciauskas and J. Peters. Polynomial C^2 spline surfaces guided by rational multisided patches. In Tor Dokken B. Jüttler, editor, *Computational Methods for Algebraic Spline Surfaces, Sept 29 – Oct 3 2003, Kefermarkt, Austria*, pages 119–134. Springer, 2004.

[KP07a] K. Karčiauskas and J. Peters. Concentric tesselation maps and curvature continuous guided surfaces. *Computer Aided Geometric Design*, 24(2):99–111, Feb 2007.

[KP07b] K. Karčiauskas and J. Peters. Guided C^2 spline surfaces with V-shaped tessellation. In J. Winkler and R. Martin, editors, *Mathematics of Surfaces*, pages 233–244, 2007.

[KP09a] K. Karčiauskas and J. Peters. Assembling curvature continuous surfaces from triangular patches. *Computers and Graphics*, 33(3):204–210, 2009.

[KP09b] K. Karčiauskas and J. Peters. Guided spline surfaces. *Computer Aided Geometric Design*, 26(1):105 – 116, 2009.

[KPR04] K. Karciauskas, J. Peters, and U. Reif. Shape characterization of subdivision surfaces – case studies. *Computer Aided Geometric Design*, 21(6):601–614, july 2004.

[Lev06] Adi Levin. Modified subdivision surfaces with continuous curvature. *ACM Trans. Graph*, 25(3):1035–1040, 2006.

[Loo04] Charles Loop. Second order smoothness over extraordinary vertices. In *Symp Geom Processing*, pages 169–178, 2004.

[LS08] Charles T. Loop and Scott Schaefer. G ^{2} tensor product splines over extraordinary vertices. *Comput. Graph. Forum*, 27(5):1373–1382, 2008.

[PBP02] Hartmut Prautzsch, Wolfgang Boehm, and Marco Paluszny. *Bézier and B-spline techniques*. Springer Verlag, 2002.

[Pet02] J. Peters. C^2 free-form surfaces of degree (3,5). *Computer Aided Geometric Design*, 19(2):113–126, 2002.

[PF09] J. Peters and Jianhua Fan. On the complexity of smooth spline surfaces from quad meshes. *Computer Aided Geometric Design*, 27:96–105, 2009.

[PK10] Jörg Peters and K. Karčiauskas. An introduction to guided and polar surfacing. In *Mathematical Methods for Curves and Surfaces*, volume 5862/2010, pages 299–315. Springer, 2010. Seventh International Conference on Mathematical Methods for Curves and Surfaces Toensberg, Norway, Toensberg, Norway, June 26-July 1, 2008, Revised Selected Papers.

[PR08] J. Peters and U. Reif. *Subdivision Surfaces*, volume 3 of *Geometry and Computing*. Springer-Verlag, New York, 2008.

[Pra97] H. Prautzsch. Freeform splines. *Comput. Aided Geom. Design*, 14(3):201–206, 1997.

[Rei98] U. Reif. TURBS—topologically unrestricted rational B-splines. *Constr. Approx.*, 14(1):57–77, 1998.

[Ye97] Xiuzi Ye. Curvature continuous interpolation of curve meshes. *Computer Aided Geometric Design*, 14(2):169–190, 1997.

[YZ04] Lexing Ying and Denis Zorin. A simple manifold-based construction of surfaces of arbitrary smoothness. *ACM TOG*, 23(3):271–275, August 2004.